RESEARCH ARTICLE OPEN ACCESS

Spectral Analysis of Sm^{3+}& Dy^{3+}: B_2O_3-Zno-Mgo Optical Glasses

M. Venkateswarlu*, V. Naresh, R. Ramaraghavulu, B.H. Rudramadevi and S. Buddhudu
Department of Physics, Sri Venkateswara University, Tirupati 517 502, India

ABSTRACT
The present paper reports on the spectral results pertaining to Sm^{3+} or Dy^{3+} (0.2 mol%) ions doped B_2O_3-ZnO-MgO (BZM) glasses. The amorphous nature of the reference glass ($65B_2O_3$-20ZnO-15MgO) has been confirmed from its XRD measurement. Thermal analysis has been carried out for the precursor chemical mix and its weight loss has been noticed from the TG profile. Based on the DTA profile, the precursor chemicals mix transition temperature (T_g) and crystallization temperature (T_c) have been identified. The transformation of trigonal BO_3 units into tetrahedral BO_4 units has evidenced from the Fourier transform infrared (FTIR) spectrum of reference glass without dopant ion(s). Spectral measurements of absorption, excitation, emission and emission transition lifetimes have been carried out for the Sm^{3+} and Dy^{3+} ions containing BZM glasses separately. These glasses exhibit strong intense absorption bands in the near-infrared (NIR) region. The emission spectrum of Sm^{3+}: BZM glass shows a prominent and bright orange-red emission at 602 nm ($^4G_{5/2} \rightarrow {}^6H_{7/2}$) upon excitation with λ_{exci} = 404 nm ($^6H_{5/2} \rightarrow {}^4F_{7/2}$). In the case of Dy^{3+}: BZM glass, an appreciable blue emission at 485 nm ($^4F_{9/2} \rightarrow {}^6H_{15/2}$) has been identified with an excitation at λ_{exci} = 387 nm ($^6H_{15/2} \rightarrow {}^4I_{13/2}$). Energy level schemes relating to the emission mechanisms involved both in Sm^{3+} and Dy^{3+} glasses have also been explained. Decay curves are have been plotted in order to evaluate emission band lifetimes.
Keywords - RE^{3+} glasses, Optical analysis

I. INTRODUCTION

Trivalent rare-earth ions doped glasses are very attractive and have drawn a great deal of interest in the fields of photonics and optoelectronic materials development [1]. The optical properties of rare-earth ions doped glass systems like silicates, phosphates, borates, germanates, tellurites, fluorides, etc have earlier been reported in the literature [2-17]. The study of environment around the rare-earth ion has been viewed necessary to understand the optical absorption and luminescent properties of rare-earth ion-doped glasses. Borate glasses are considered to be structurally more encouraging and found them as good candidates in doping them with varied amounts of rare earth ions in tailoring the optical materials suitable to the purpose meant for when compared with silicate or phosphate glasses because of the existence of coordination of boron atoms with oxygens. The structure of the borate glasses consists of a random network of boroxol rings and BO_3 triangles connected by B-O-B linkage (bridging oxygen atom). The addition of alkali oxides (as modifiers) could transform the boroxol ring into four coordinated boron atoms, BO_4 tetrahedra. [14].

With the presence of property modifying salts like ZnO + MgO with B_2O_3 glass network could significantly improve different properties like very glass nature, mechanical strength and thermal stability with an extended chemical durability. Such glasses could be found as more supportive materials for their applications in optical communications (optical fibers), laser hosts, optical filters, γ-ray absorbers, photonic devices etc [18-24]. Keeping in view the applications of alkaline earth borate glasses containing heavy metal oxides, the present work has been undertaken to study both absorption and photoluminescence spectra properties of Sm^{3+} ($4f^5$) and Dy^{3+} ($4f^9$) ions each separately doped in them, since their display of strong absorption bands in the NIR wavelengths (800-2200 nm) and intense emission bands in the visible (450-750 nm) region.

II. EXPERIMENTAL STUDIES

2.1. GLASS PREPARATION

The borate zinc magnesium (BZM) glasses in the follwoing chemical composition containing Sm^{3+} or Dy^{3+} ions in 0.2 mol % each separately, along with a host glass as well:

i. *Host glass:* $65B_2O_3$-20ZnO-15MgO,
ii. *Sm^{3+}: BZM:* $64.8B_2O_3$-20ZnO-15MgO, &
iii. *Dy^{3+}: BZM:* $64.8B_2O_3$-20ZnO-15MgO.

The starting materials used in the present work were reagent grade of H_3BO_3, $ZnCO_3$, $MgCO_3$, Sm_2O_3 and Dy_2O_3. All weighted chemicals were powdered finely and mixed thoroughly before each batch (10g) was melt in porceline crucibles in an electrical furnace for an hour, at 980 ^{0}C. These melts were quenched in between two brass plates to obtain 2-3 cm diameter optical glass discs of 0.3 cm thickness. These glasses thus obtained were used for further characterizations. **Fig. 1** displays the glasses developed in the present work.

2.2. MEASUREMENTS

Powder X-ray diffraction (XRD) spectra were obtained on a Shimadzu XD 3A diffractometer with a Ni filter and Cu-K_α (1.5418A°) radiation with an applied voltage of 30 KV and 20 mA anode current, calibrated with Si and at a scanning rate of 2^o min^{-1}. Thermal analysis for the precursor chemicals of host composition were carried out on a NetZsch STA 409 system from room temperature to 800 ºC at a heating rate of 10 ºC/min under N_2 gas atmosphere. The FT-IR spectrum (4000-450 cm^{-1}) was recorded on a Nicolet IR-200 Spectrophotometer with KBr pellet technique. The optical absorption spectra were measured on a Varian-Cary Win spectrometer (JASCO V-570). The excitation and emission spectra were obtained on a SPEX Fluorolog-2 Fluorimeter (Model-II) with Data max software to acquire the data with Xe-flash lamp (150W) as the excitation source. A Xe-flash lamp with a phosphorimeter attachment was used to measure the lifetimes of the emission transitions of Sm^{3+} and Dy^{3+} glasses.

III. RESULTS AND DISCUSSION

3.1. HOST GLASS

The measured X-ray diffraction (XRD) profile of the host glass ($65B_2O_3$-20ZnO-15MgO) is shown in **Fig. 2**, which confirms its amorphous (vitreous state) nature. In **Fig. 3**, simultaneous measurement of thermogravimetric (TG) and differential thermal analysis (DTA) for the host $65B_2O_3$-20ZnO-15MgO precursor chemical mix in the temperature range of 30 ºC to 800 ºC is shown. From TG profile, it is observed that the weight loss of the sample takes in a multistep process. The initial weight loss of sample about 5% is noticed between 30 ºC and 126 ºC due to the decomposition of the organic compounds used during the grinding of the chemical mix for homogeneity and dehydration of water. The second weight loss is noticed in the temperature range of 126 ºC – 213 ºC, due to the transformation of boric acid H_3BO_3 into HBO_2; with a weight loss of 3%. Upon further heating, the third weight loss has occurred in the temperature range of 213 ºC – 335 ºC because of the conversion of HBO_2 as an anhydrous oxide B_2O_3 in crystalline form that melts at 335 ºC, the corresponding weight loss is observed to be 7%. The final weight loss is observed in the range of 335 ºC–700 ºC, due to the decomposition of $ZnCO_3$ into ZnO and CO_2; $MgCO_3$ into MgO and CO_2 which is about 15 %. No significant weight loss has been noticed beyond 700 ºC as seen from the TG profile of the BZM glass precursor chemicals [25]. The point of slope change of endothermic peak in DTA curve at 325 ºC indicates the glass transition temperature (T_g) as marked in the DTA profile. The exothermic peak at 430 ºC is identified to be crystallization temperature (T_c). Glass stability factor has been measured from the T_g and T_c values of DTA curve by using the relation, glass stability factor (S) = T_c - T_g, it is found to be 105 ºC.

FT-IR spectral study was carried out to identify the local structure and functional groups. The FT-IR spectrum of the reference (BZM) glass is shown **Fig. 4**. The structure of borate glasses consists of random network of BO_3 triangles with certain fractions of boroxol (six membered) rings. In the infrared range, the vibrational modes of the borate network have three regions. Accordingly, the bands in the first region 1200-1600 cm^{-1}, arises due to an asymmetric stretching relaxation of the B-O bond of trigonal BO_3 units, the second region located at 800-1200 cm^{-1} which is due to the B-O bond stretching of tetrahedral BO_4 units, and the third region around 700 cm^{-1} which is because of the bending of B-O-B linkages in the borate network [26]. Vibrational bands around 3451, 2924, 2850, 1359, 1221, 1020 and 707 cm^{-1} are observed in the FT-IR spectrum. The broad band around 3451 cm^{-1} is ascribed to a hydroxyl (or) water group originating from molecular water. Two IR bands at ~2924 and ~2850 cm^{-1} are indicative of hydrogen bonding. The band around 1359 and 1221 cm^{-1} is characteristic of the B-O stretching vibrations of trigonal $(BO_3)^{3-}$ units in metaborate, pyroborate and orthoborate groups. The peak around 1020 cm^{-1} is attributed to the B-O bond stretching of BO_4 units. The absorption band around 707 cm^{-1} indicates the bending of B-O-B linkage in the borate network [1]. In general, the absorption band at 806 cm^{-1} is attributed to the boroxol ring in the borate glass network.

In the present study, the peak at 806 cm^{-1} could not be found, which indicates the absence of boroxol ring in the glass network due transformation of BO_3 triangles into BO_4 tetrahedrals.

3.2. Sm^{3+} GLASS

The UV-VIS and NIR absorption spectra of Sm^{3+}: BZM glass are shown in **Fig. 5 (a & b)**, with intense absorption bands in the NIR region. All

transitions in the absorption spectrum of Sm^{3+} are intra-configurational (f-f) transitions and originate from the ground state $^6H_{5/2}$ to the various higher states [3]. The observed absorption bands are assigned to electronic transitions of $^6H_{5/2} \rightarrow {}^4F_{7/2}$, $^4G_{9/2}$, $^4I_{11/2}$, $^4F_{3/2}$, $^4G_{5/2}$, $^6F_{11/2}$, $^6F_{9/2}$, $^6F_{7/2}$, $^6F_{5/2}$, $^6F_{3/2}$, $^6H_{15/2}$ and $^6F_{1/2}$ at 402 nm, 437 nm, 471 nm, 534 nm, 586 nm, 933 nm, 1073 nm, 1221 nm, 1367 nm, 1472 nm, 1528 nm and 1576 nm, respectively [27]. The majority of the transitions in the spectra are due to induced electric dipole interactions with selection rule $\Delta J \leq 6$ and also due to magnetic dipole contribution with selection rule $\Delta J = 0, \pm 1$. In the visible region, all the transitions are spin forbidden and hence, the absorption bands are weak in intensity. The transitions from ground $^6H_{5/2}$ state to ^6H_J and ^6F_J states are spin allowed ($\Delta S=0$) hence, these transitions lying in the NIR region (<11,000 cm^{-1}) are intense and distinctly sharp due to the effective shielding of 4f electrons by the filled 5s and 5p shells [14]. **Fig. 6** represents excitation spectrum of Sm^{3+}: BZM glass, with seven excitation bands of $^6H_{5/2} \rightarrow {}^4H_{9/2}$, $^6H_{5/2} \rightarrow {}^4D_{3/2}$, $^6H_{5/2} \rightarrow {}^6P_{7/2}$, $^6H_{5/2} \rightarrow {}^4F_{7/2}$, $^6H_{5/2} \rightarrow (^6P_{5/2}, {}^4P_{5/2})$, $^6H_{5/2} \rightarrow {}^4G_{9/2}$ and $^6H_{5/2} \rightarrow {}^4I_{11/2}$ at 345 nm, 362 nm, 375 nm, 404 nm, 418 nm, 439 and 471nm respectively. Among these, a prominent excitation band at 404 nm has been selected for the measurement of emission spectrum of Sm^{3+} glass. When the $^4F_{7/2}$ level (404 nm) of Sm^{3+} is excited, the Sm^{3+} ions in the higher excited state decay noradiatively to the $^4G_{5/2}$ level by populating it. On reaching $^4G_{5/2}$ metastable state, unstable ions relax to the nearest lying states ^6H_J (J = 5/2, 7/2, 9/2 and 11/2) by depopulating it with emission of fluorescence [28]. **Fig. 7** represents emission spectrum of Sm^{3+}: BZM glass, with four emission transitions of $^4G_{5/2} \rightarrow {}^6H_{5/2}$ (565 nm), $^4G_{5/2} \rightarrow {}^6H_{7/2}$ (602 nm), $^4G_{5/2} \rightarrow {}^6H_{9/2}$ (648 nm) and $^4G_{5/2} \rightarrow {}^6H_{11/2}$ (708 nm) transitions. Of these transitions, $^4G_{5/2} \rightarrow {}^6H_{7/2}$ (602 nm) has shown a strong emission in orange-red region. The Sm^{3+} glass exhibiting bright *orange-red* colour under an UV source is shown in the inset of Fig.7. The transition $^4G_{5/2} \rightarrow {}^6H_{7/2}$ with $\Delta J = \pm 1$ is a magnetic dipole (MD) allowed but it is an electric dipole (ED) dominated, and the other transition $^4G_{5/2} \rightarrow {}^6H_{9/2}$ is purely an electric dipole (ED) transition [3, 28]. Generally the intensity ratio between ED and MD transition has been be used to measure the symmetry of the local environment of the trivalent 4f ions. The greater the intensity of the ED transitions more is the asymmetry nature [3]. In the present work, the transition $^4G_{5/2} \rightarrow {}^6H_{9/2}$ which is ED in nature has less intensity over the MD transition $^4G_{5/2} \rightarrow {}^6H_{5/2}$, which specifies the symmetric nature of the glass host. **Fig. 8** presents the decay curve, which is plotted for the prominent emission transition $^4G_{5/2} \rightarrow {}^6H_{7/2}$ at 602 nm with an excitation wavelength of 404 nm. The decay curve exhibited a exponential nature and its lifetime has found to be 1.57 ms. The energy level scheme involved in the emission process for Sm^{3+} glass is shown in the inset of **Fig.8.**

3.3. Dy^{3+} GLASS

The UV-VIS and NIR absorption spectra of Dy^{3+}: BZM glass are shown in **Fig. 9 (a & b)**. All the transitions in the absorption spectrum of Dy^{3+} arise from the ground state, $^6H_{15/2}$ to higher energy states. From **Fig. 9**, the levels of $^4G_{11/2}$ (425 nm), $^4I_{15/2}$ (451 nm), $^4F_{9/2}$ (475 nm), $^6F_{3/2}$ (747 nm), $^6F_{5/2}$ (798 nm), $^6F_{7/2}$ (884 nm), ($^6F_{9/2}$, $^6H_{7/2}$) (1082 nm), ($^6F_{11/2}$, $^6H_{9/2}$) (1261 nm) and $^6H_{11/2}$ (1696 nm) are well resolved [29, 30]. The position and intensity of certain transitions of rare-earth ions are found to be very sensitive to the environment around the ion. Such transitions are termed as hypersensitive transitions. These transitions obey the selection rule $|\Delta S|=0$, $|\Delta L| \leq 2$, $|\Delta J| \leq 2$ [1, 28]. In the case of Dy^{3+} ($4f^9$) ion, the hypersensitive transition ($^6F_{11/2}$, $^6H_{9/2}$) is found to be more intense than the other transitions. **Fig. 10** presents excitation spectrum of Dy^{3+}: BZM glass, which was measured by monitoring an intense emission at 485 nm. The excitation spectrum exhibited seven bands assigned to the electronic transitions with the ground state $^6H_{15/2}$ to higher energy levels of Dy^{3+} , i.e., $^6H_{15/2} \rightarrow {}^6P_{3/2}$ (325 nm), $^6H_{15/2} \rightarrow {}^6P_{7/2}$ (351 nm), $^6H_{15/2} \rightarrow {}^4P_{3/2}$ (365 nm), $^6H_{15/2} \rightarrow {}^4F_{7/2}$ (387 nm), $^6H_{15/2} \rightarrow {}^4G_{11/2}$ (426 nm), $^6H_{15/2} \rightarrow {}^4I_{15/2}$ (453 nm) and $^6H_{15/2} \rightarrow {}^4F_{9/2}$ (473 nm) [27,29]. From these excitation transitions, a prominent transition at 387 nm has been selected for the measurement of emission spectrum of Dy^{3+}glass. When the ($^4F_{7/2}$) level of Dy^{3+} is excited with 387 nm, Dy^{3+} ions in the higher energy state decay nonradiatively to $^4F_{9/2}$ state and populates it. Upon reaching this state, ions relax to the lower lying states of ^6H_J revealing fluorescence [31]. **Fig. 11** presents the emission spectrum of Dy^{3+}: BZM glass exhibiting three emission transitions of $^4F_{9/2} \rightarrow {}^6H_{15/2}$ (485 nm), $^4F_{9/2} \rightarrow {}^6H_{13/2}$ (577 nm) and $^4F_{9/2} \rightarrow {}^6H_{11/2}$ (670 nm) for blue, yellow and red regions. Among these three transitions, the $^4F_{9/2} \rightarrow {}^6H_{15/2}$ (blue) is magnetic dipole (MD) transition possessing higher intensity, $^4F_{9/2} \rightarrow {}^6H_{11/2}$ (red) possessing lower intensity and $^4F_{9/2} \rightarrow {}^6H_{13/2}$ (yellow) transition possessing moderate intensity related to the electric dipole (ED) transition. The intensity ratio of ED to MD transitions has been used to measure the symmetry of the local environment of the trivalent 4f ions. In the present work, $^4F_{9/2} \rightarrow {}^6H_{13/2}$ (ED) transition of Dy^{3+} ions is less intense than $^4F_{9/2} \rightarrow {}^6H_{15/2}$ (MD), revealing the symmetry nature of studied glass. **Fig. 12** presents the decay curve, which is plotted for the prominent emission transition $^4F_{9/2} \rightarrow {}^6H_{15/2}$ at 485 nm with an excitation at 387 nm. The decay curve has exhibited a

non-exponential feature with a lifetime of 0.57 ms. The energy level scheme involved in the emission process Dy^{3+} ions has been indicated as an inset in **Fig. 12**.

IV. CONCLUSION

In summary, it is concluded that we have successfully developed transparent, moisture resistant and stable (0.2 mol %) and brightly luminescent Sm^{3+} and Dy^{3+}: $64.8B_2O_3$-20ZnO-15MgO glasses, for their Spectral analysis systematically. The amorphous nature of host (BZM) glass has been confirmed from its XRD profile. The weight loss, transition temperature (T_g) and crystallization temperature (T_c) have been noticed and identified from TG-DTA profiles of host precursor chemical mix. The FTIR spectrum has revealed transformation of BO_3 triangles into BO_4 tetrahedral. VIS-NIR absorption spectra of these glasses have been analyzed. Emission spectrum of Sm^{3+} glass has shown four emission transitions, $^4G_{5/2}\rightarrow{}^6H_{5/2}$ (565 nm), $^4G_{5/2}\rightarrow{}^6H_{7/2}$ (602 nm), $^4G_{5/2}\rightarrow{}^6H_{9/2}$ (648 nm) and $^4G_{5/2}\rightarrow{}^6H_{11/2}$ (708 nm) with an excitation at 404 nm $^6H_{5/2}\rightarrow{}^4F_{7/2}$ and Dy^{3+} glass has shown three emission transitions $^4F_{9/2}\rightarrow{}^6H_{15/2}$ (485 nm), $^4F_{9/2}\rightarrow{}^6H_{13/2}$(577 nm) and $^4F_{9/2}\rightarrow{}^6H_{11/2}$ (670 nm) upon excitation at 387 nm ($^6H_{15/2}\rightarrow{}^4F_{7/2}$). Sm^{3+} and Dy^{3+} glasses have shown bright orange and blue emissions under an UV source. The decay curves of the emission transition ($^4G_{5/2}\rightarrow{}^6H_{7/2}$) of Sm^{3+} and ($^4G_{5/2}\rightarrow{}^6H_{7/2}$) of Dy^{3+} have been found to be at 1.57 ms and at 0.57 ms respectively. Based on the above results, these glasses could be suggested as interesting optical luminescent materials with technological importance.

REFERENCES

[1] R.T. Karunakaran, K. Marimuthu, S. Surendra Babu and S. Arumugam, Dysprosium doped alkali fluroborate glasses-thermal, structural and optical investigations, *J. Lumin.* **130,** 2010, 1067-1072.

[2] Y. K. Sharma, S.S.L. Surana and R.K. Singh, Spectroscopic investigations and luminescence spectra of Sm^{3+} doped soda lime silicate glasses, *J. Rare Earths* **27,** 2009, 773-780.

[3] L. Zhu, C. Zuo, Z. Luo and A. Lu, Photoluminescence of Dy^{3+} and Sm^{3+}: SiO_2-Al_2O_3-LiF-CaF_2 glasses, *Physica B* **405,** 2010, 4401-4406.

[4] P. Chimalawong, K. Kirdsiri, J. Kaewkhao and P. Limsuwan, Investigation on the Physical and Optical Properties of Dy^{3+} Doped Soda-Lime-Silicate Glasses, *Procedia Eng.* **32,** 2012, 690-698.

[5] I. Pal, A. Agarwal, S. Sanghi and M.P. Agarwal, Investigation of spectroscopic properties, structure and luminescence spectra of Sm^{3+} doped zinc bismuth silicate glasses, *Spectrochim. Acta A* **101**, 2013, 74-81.

[6] P. Raghava Rao, G. Murali Krishna, M.G. Brik, Y. Gandhi and N. Veeraiah, Fluorescence features of Sm^{3+} ions in Na_2SO_4-MO-P_2O_5 glass system-Influence of modifier oxide, *J. Lumin.* **131,** 2011, 212-217.

[7] J. Pisarska, Luminescence behavior of Dy^{3+} ions in led borage glasses, *Opt. Mater.* **31,** 2009, 1784-1786.

[8] A.A. Ali, Optical properties of Sm^{3+} - doped CaF_2 bismuth borate glasses, *J. Lumin.* **129,** 2009, 1314-1319.

[9] J.A. Pisarska, L. Zur and W. A. Pisarski, Visible luminescence of dysprosium ions in oxyhalide lead borate glasses, *Spectrochim. Acta A* **79,** 2011, 705-707.

[10] I. Pal, A. Agarwal, S. Sanghi and M.P. Aggarwal, Structure and optical absorption of Sm^{3+} and Nd^{3+} ions in cadmium bismuth borate glasses with large radiative transition probabilities, *Opt. Mater.* **34,** 2012, 1171-1180.

[11] M. Jayasimhadri, Eun-Jin Cho, Ki-Wan Jang, Ho Sueb Lee and Sun Il kim, Spectroscopic properties and Judd-Ofelt analysis of Sm^{3+} doped lead-germanate-tellurite glasses, *J. Phys. D: Appl. Phys.* **41,** 2008, 175101-175107.

[12] L. Zur, Structural and luminescence properties of Eu^{3+}, Dy^{3+} and Tb^{3+} ions in lead germanate glasses obtained by conventional high-temperature melt-quenching technique, *J. Mol. Struct.* **1041,** 2013, 50–54.

[13] K. Maheshvaran, K.Linganna and K.Marimuthu, Composition dependent structural and optical properties of Sm^{3+} doped boro-tellurite glasses, J. *Lumin.* **131,** 2011, 2746-2753.

[14] S. Shanmuga Sundari, K. Marimuthu, M. Sivaraman and S. Surendra Babu, Composition dependent structural and optical properties of Sm^{3+} -doped sodium borate and sodium fluoroborate glasses, *J. Lumin.* **130,** 2010, 1313-1319.

[15] I. Arul Rayappan, K. Selvaraju and K. Marimuthu, Structural and luminescence investigations on Sm^{3+} doped sodium fluoroborate glasses containing

alkali/alkaline earth metal oxides, *Physica B* **406,** 2011, 548-555.

[16] I. Arul Rayappan, K. Marimuthu, S. Surendra Babu and M. Sivaraman, Concentration dependent structural, optical and thermal investigations of Dy^{3+} -doped sodium fluoroborate glasses, *J. Lumin.* **130,** 2010, 2407-2412.

[17] K. Gatterer, G. Pucker, H.P. Fritzer and S. Arafa, Hypersensitivity and nephelauxetic effect of Nd(III) in sodium borate glasses, *J. Non-Cryst. Solids* **176,** 1994, 237-246.

[18] F.H. El-Batal, M.A. Azooz and F.M. Ezz-Eldin, Thermal expansion and infrared studies of binary Bi_2O_3-B_2O_3 and ternary Bi_2O_3-B_2O_3-PbO glasses, *Phys. Chem. Glasses* **43,** 2002, 260-266.

[19] G. Senthil Murugan, E. Fargin, V. Rodriguez, F. Adamirtz, M. Couzi, T. Buffeteau and P. Le Coustumer, Temperature–assisted electrical poling of TeO_2-Bi_2O_3-ZnO glasses for non-linear optical applications, *J. Non-Cryst. Solids* **344,** 2004, 158-166.

[20] G.D. Khattak, N. Tabet and L.E. Wenger, Structural properties of glasses in the series $(SrO)_x(V_2O_5)_{1-x}$, $(SrO)_{0.5-y}(B_2O_3)_y(V_2O_5)_{0.5}$, and $(SrO)_{0.2}(B_2O_3)_z(V_2O_5)_{0.8-z}$, *Phys. Rev. B* **72,** 2005, 104203-104214.

[21] S.Murugavel and B. Roling, Ion transport mechanism in borate glasses: Influence of network structure on non-Arrhenius conductivity, *Phys. Rev. B* **76,** 2007, 180202-180205.

[22] Dimitrij Lezal, Jitka Pedlikova, Petr Kostka, Jana Bludska, Marcel Poulain and Jiri Zavadil, Heavy metal oxide glasses: preparation and physical properties, *J. Non-Cryst. Solids* **284,** 2001, 288-295.

[23] J. Lin, W. Huang, Z. Sun, C. S. Ray and D. E. Day, Structure and non-linear optical performance of TeO_2–Nb_2O_5–ZnO glasses, *J. Non-Cryst. Solids* **336**, 2004, 189-194.

[24] W.H. Dumbaugh and J.C. Lapp, Heavy-Metal oxide glasses, *J. Am. Ceram. Soc.* **75,** 1992, 2315-2326

[25] V. Naresh and S.Buddhudu, Structural, thermal, dielectric and ac conductivitiy properties of lithium fluoro-borate optical glasses, *Ceram. Int.* **38,** 2012, 2325-2332.

[26] A. Thulasiramudu and S. Buddhudu, Optical characterization of Cu^{2+} ion-doped zinc lead borate glasses, *J. Quant. Sepectrosc. Radiat. Transfer* **97,** 2006, 181-194.

[27] W.T. Carnall, P.R. Fields and K. Rajnak, Electronic Energy Levels in the Trivalent Lanthanide Aquo Ions. I. Pr^{3+}, Nd^{3+}, Pm^{3+}, Sm^{3+}, Dy^{3+}, Ho^{3+}, Er^{3+}, and Tm^{3+}, *J. Chem. Phys.* **49**, 1968, 4424-4442.

[28] A. Thulasiramudu and S. Buddhudu, Optical characterization of Sm^{3+} and Dy^{3+}: ZnO-PbO-B_2O_3 glasses, *Spectrochim. Acta A* **67,** 2007, 802-807.

[29] Zhang Yan, Lu Chunhua, Ni Yaru, Zhang Qitu and Xu Zhongzi, Optical Properties of Dy^{3+} Doped in Boroaluminasilicate Glasses, *J. Rare Earths* **25,** 2007, 99-103.

[30] Xing Shen, Qiuhua Nie, Tiefeng Xu, Shixun Dai, Xunsi Wang, Feifei Chen and Gaobo Yang, Optical and crystallization behavior in Dy^{3+} doped $40GeSe_2$-$25Ga_2Se_3$-35CsI glass, *Spectrochim. Acta A* **74,** 2009, 224-227.

[31] K.K. Mahato, Anita Rai and S.B. Rai, Optical properties of Dy^{3+} doped in oxyfluoroborate glass, *Spectrochim. Acta A* **61,** 2005, 431-436.

FIGURE CAPTIONS

Fig. 1. Display of host (BZM) glass, Sm^{3+} and Dy^{3+} (0.2 mol%) ions doped BZM glasses.
Fig. 2. XRD profile of the host BZM glass.
Fig.3. TG profile of the BZM glass precursor chemicals (in inset figure DTA curve).
Fig. 4. FTIR spectrum of the host BZM glass.
Fig. 5. Absorption spectrum of Sm^{3+}: BZM glass (a) UV-Visible and (b) NIR regions.
Fig. 6. Excitation spectrum of Sm^{3+}: BZM glass.
Fig. 7. Emission spectrum of Sm^{3+}: BZM glass.
Fig. 8. Emission decay curve for emission transition of Sm^{3+}: BZM glass ((inset figure shows an energy level diagram of Sm^{3+} ions).
Fig. 9. Absorption spectrum of Dy^{3+}: BZM glass (a) UV-Visible and (b) NIR regions
Fig. 10. Excitation spectrum of Dy^{3+}: BZM glass.
Fig. 11. Emission spectrum of Dy^{3+}: BZM glass.
Fig. 12. Emission decay curve for emission transition of $Dy^{3+:}$ BZM glass (inset figure shows an energy level diagram of Dy^{3+} ions).

Figure 1

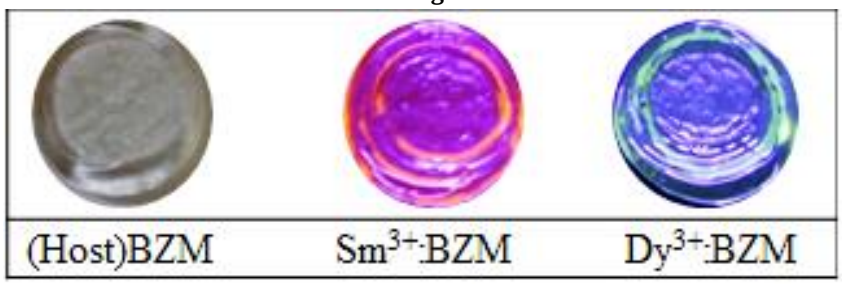

Figure 2

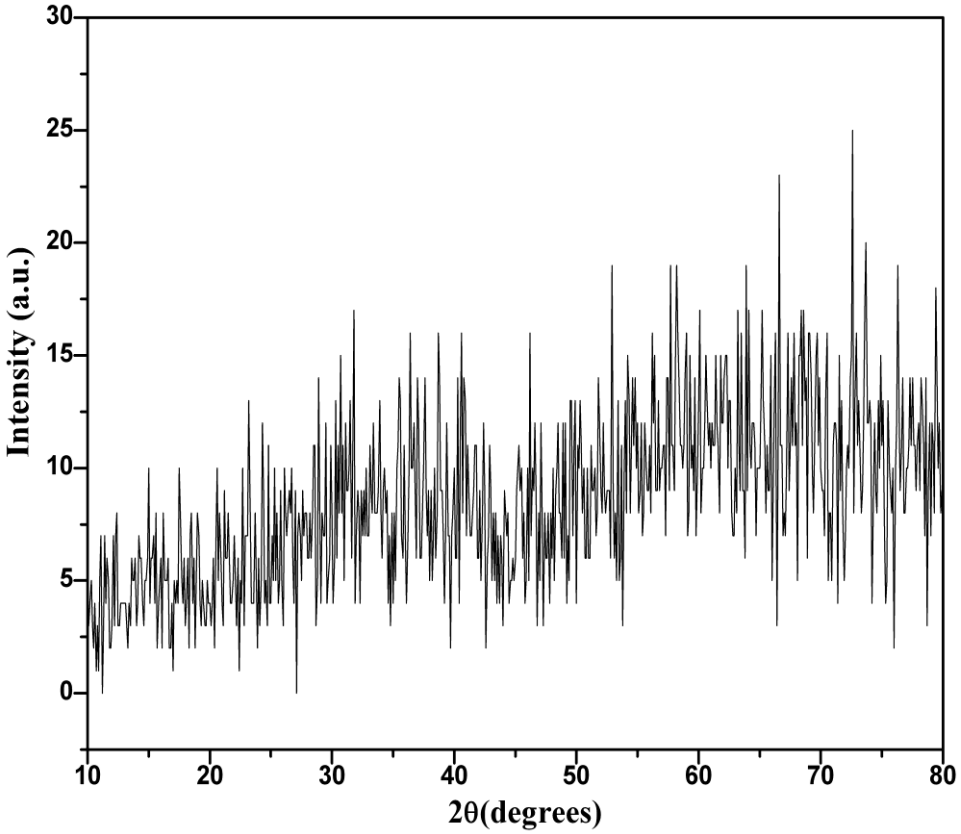

Figure 3

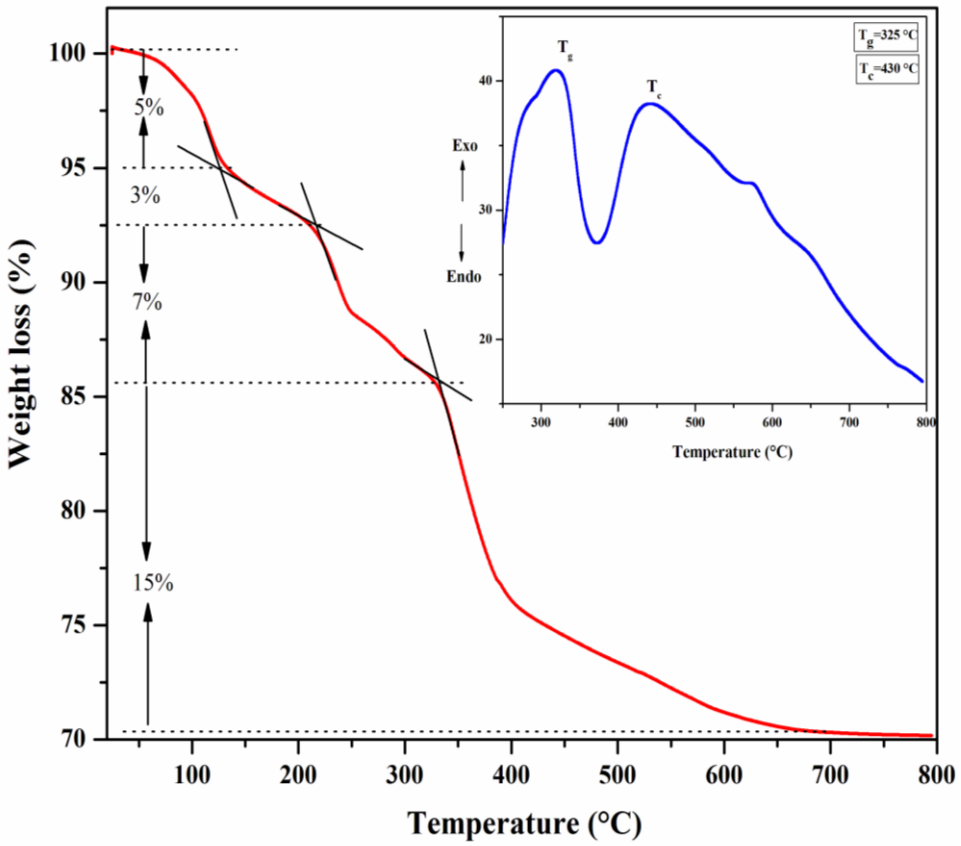

Figure 4

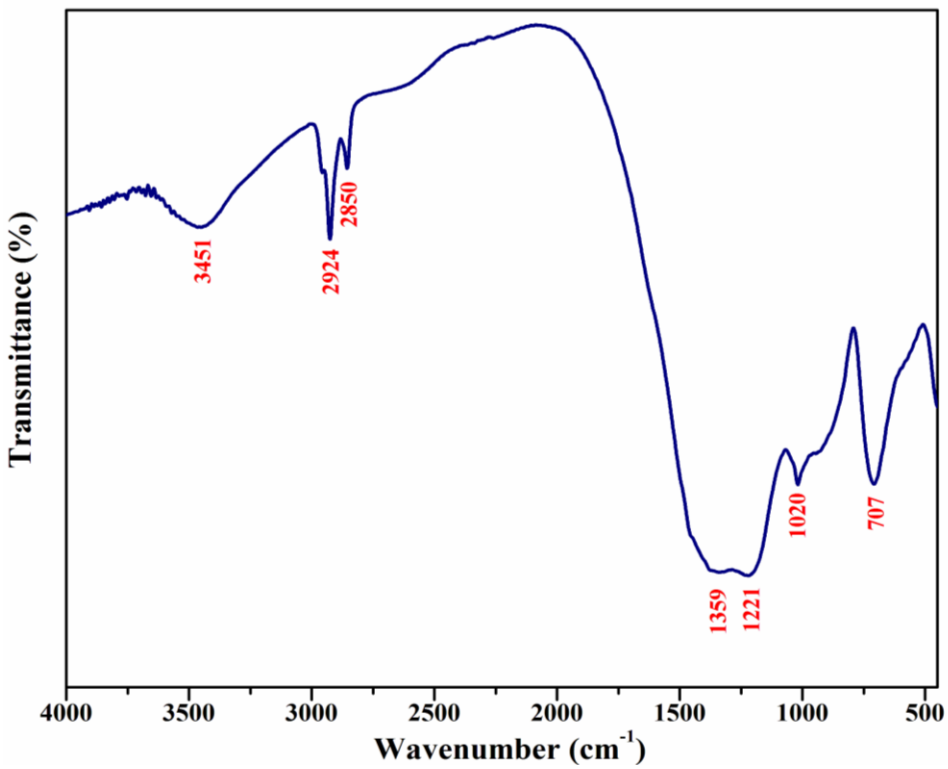

Figure 5

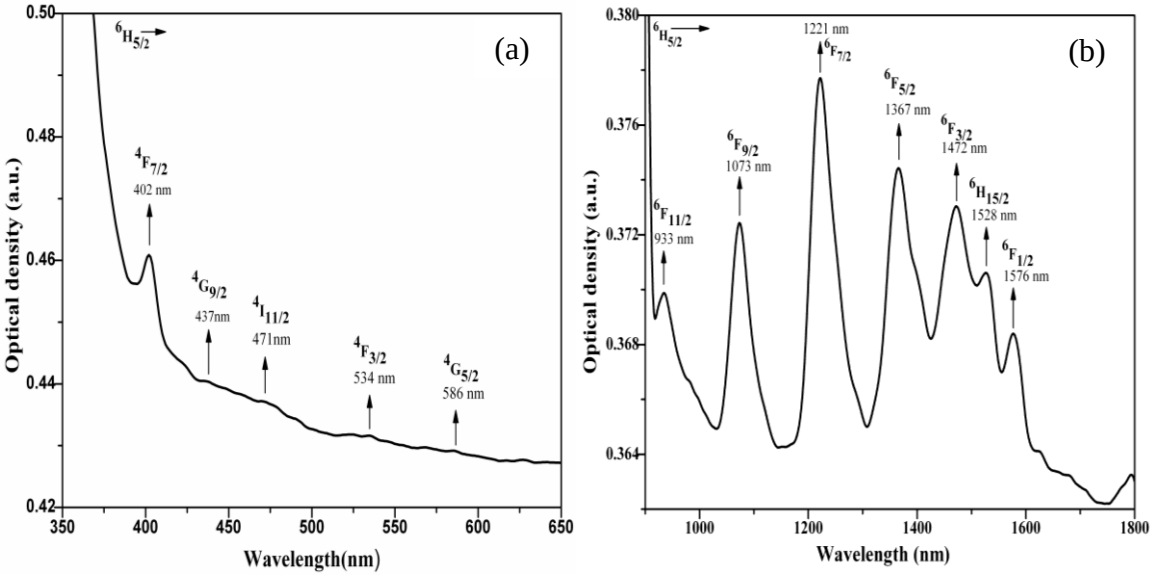

Figure 6

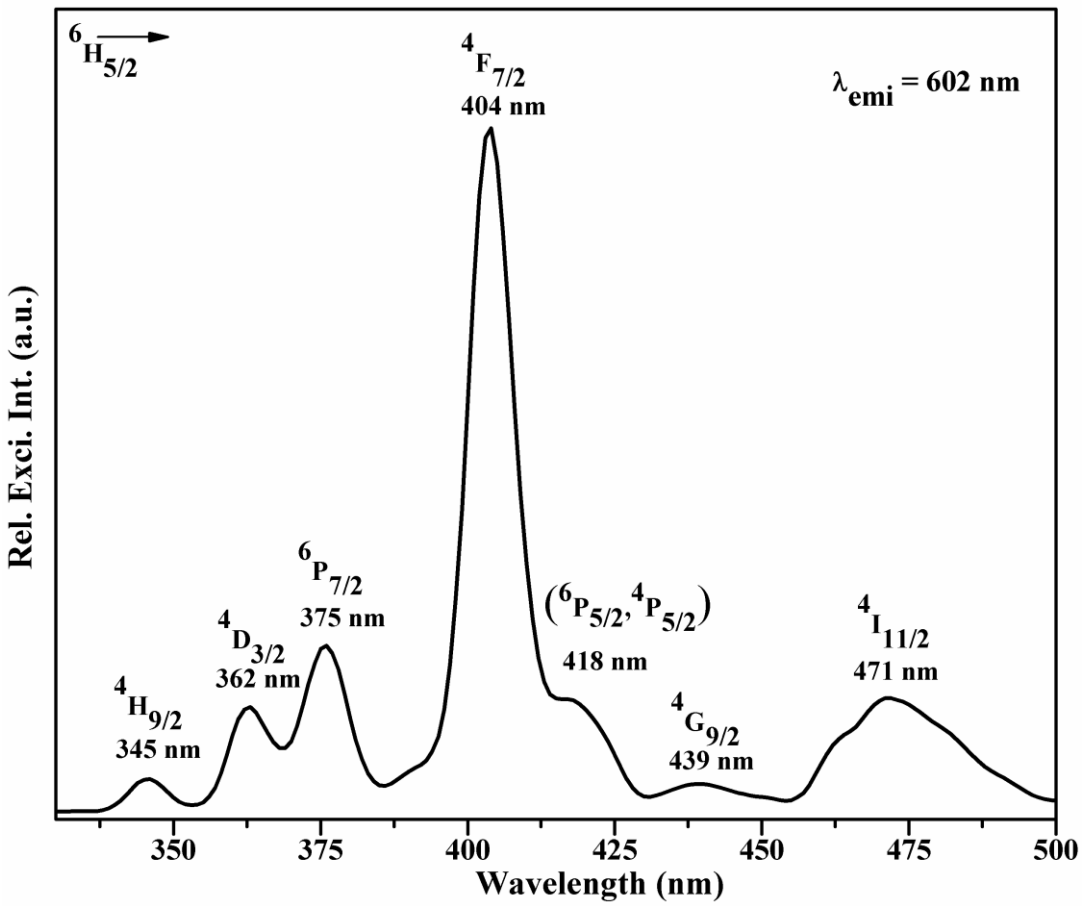

Figure 7

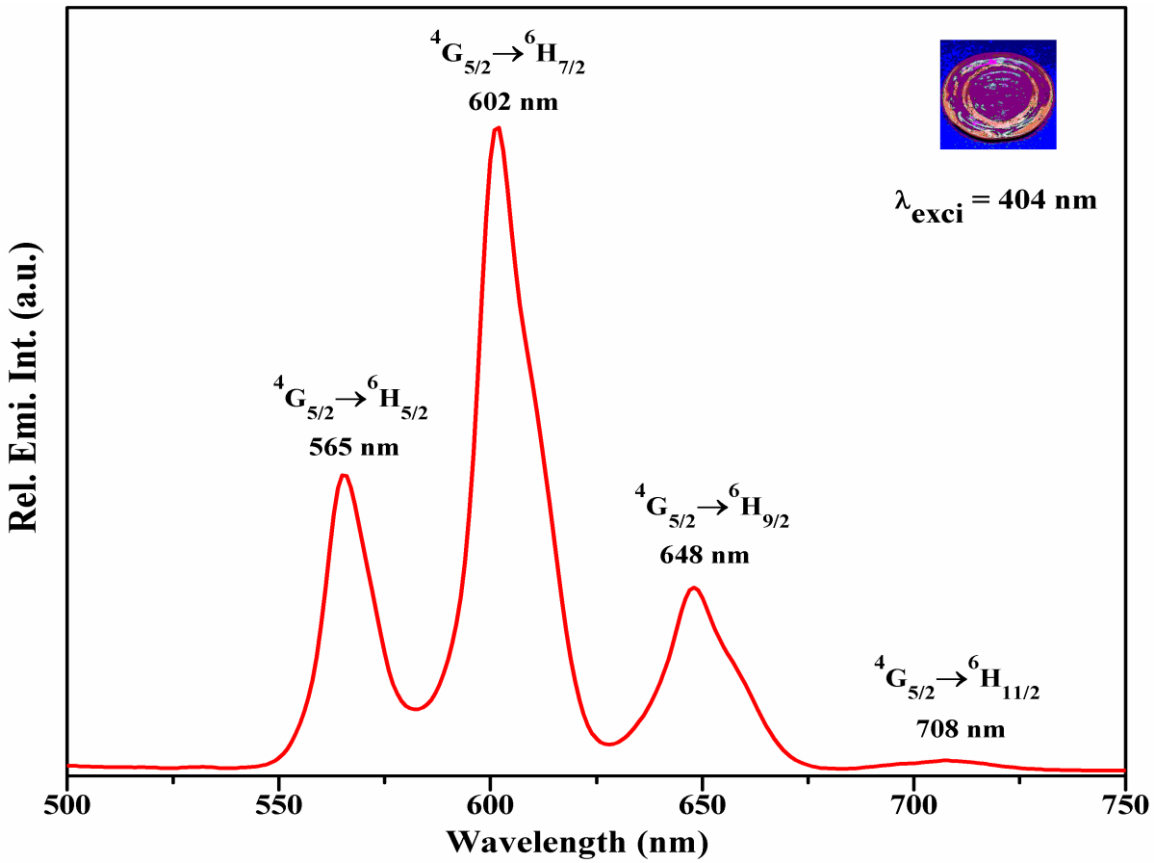

Figure 8

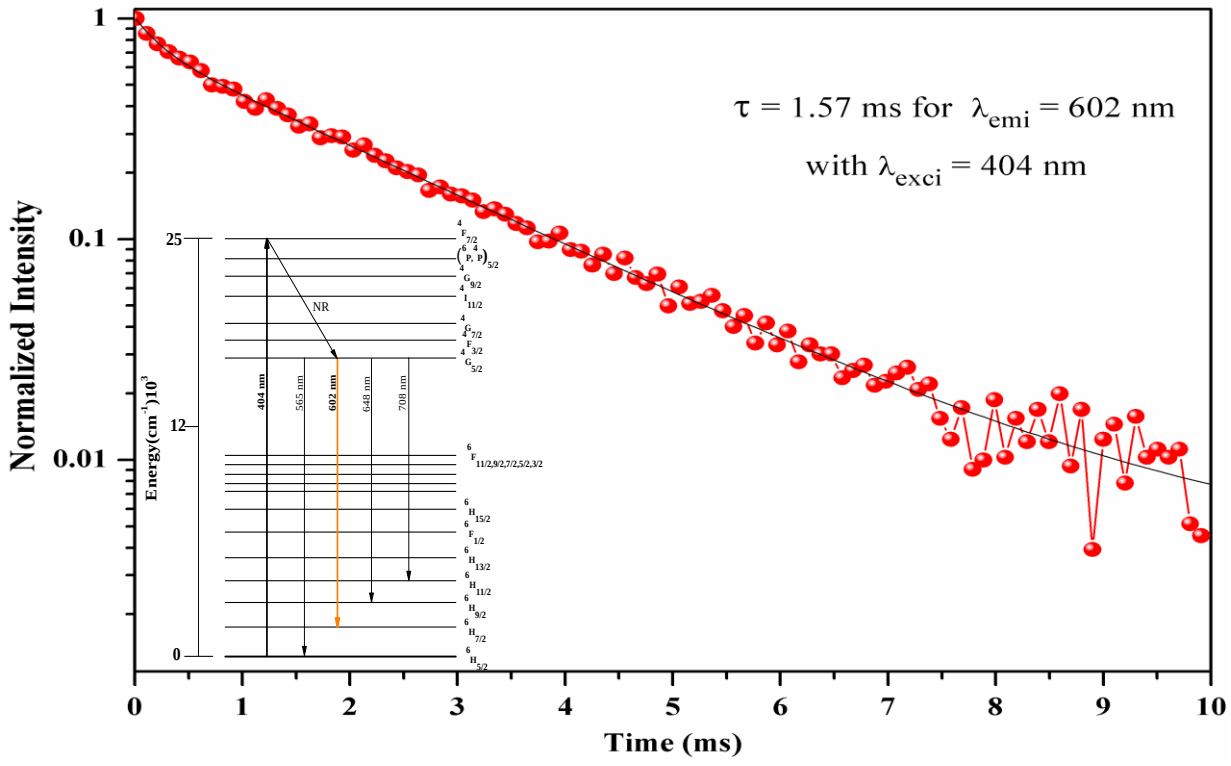

Figure 9

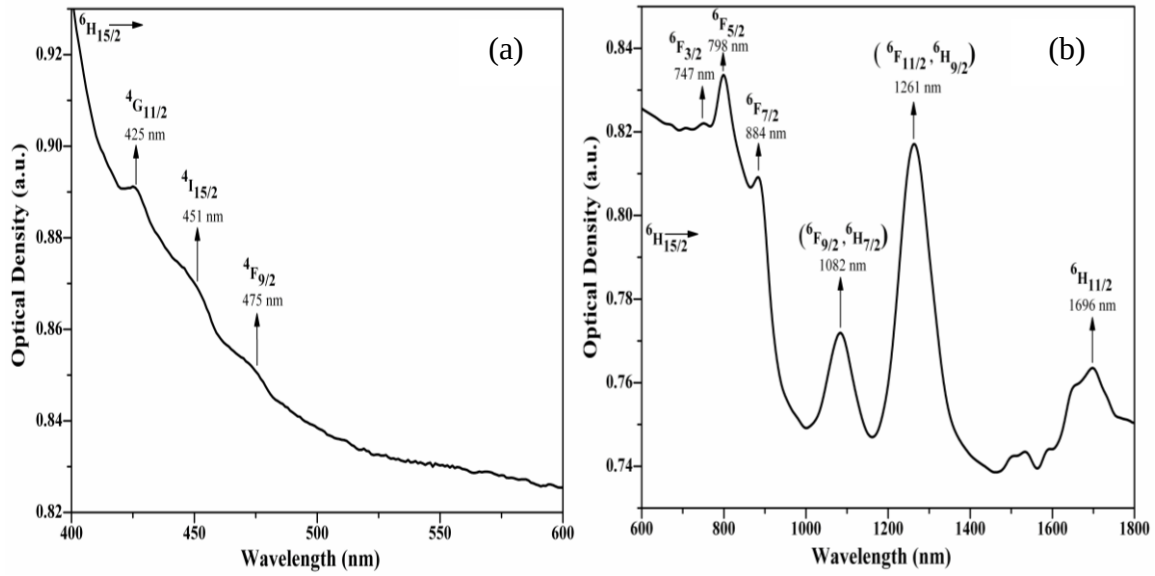

Figure 10

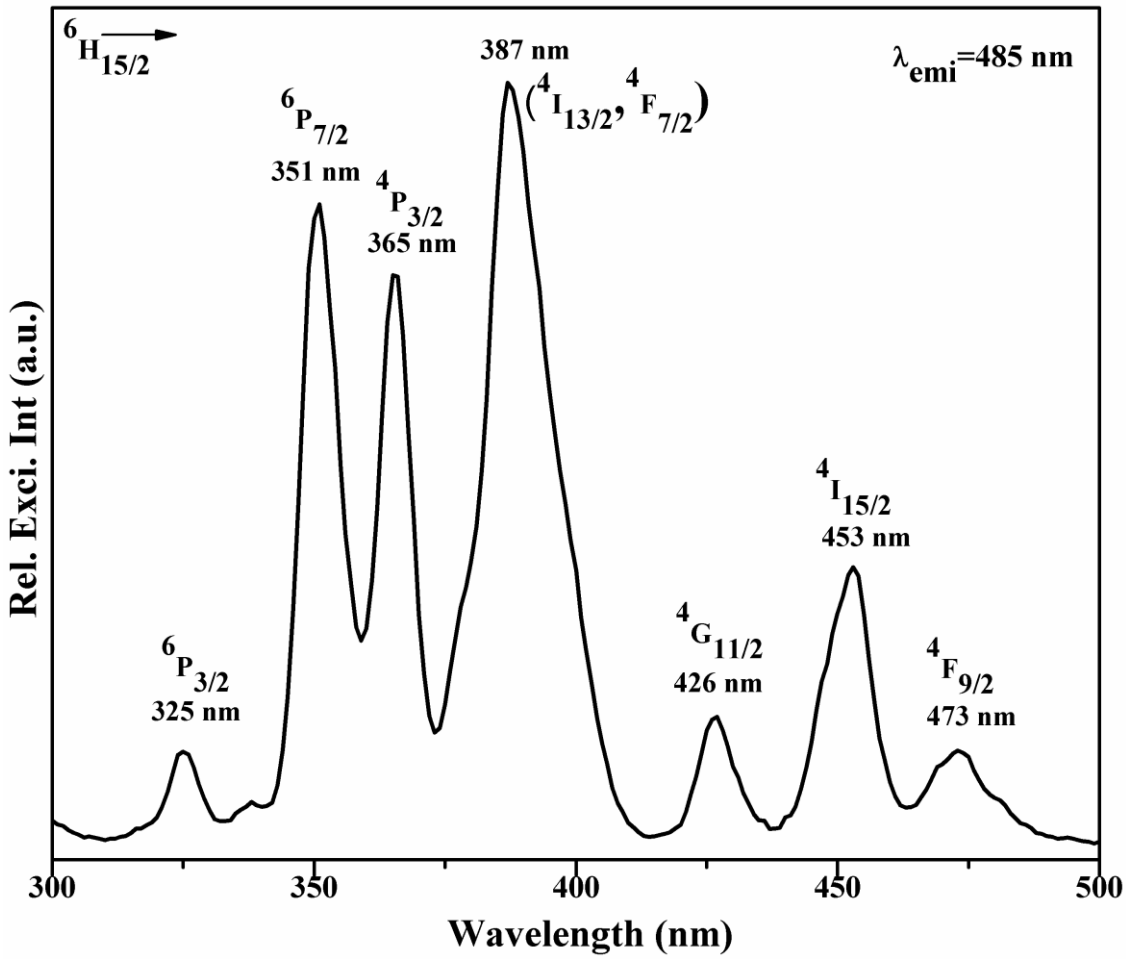

Figure 11

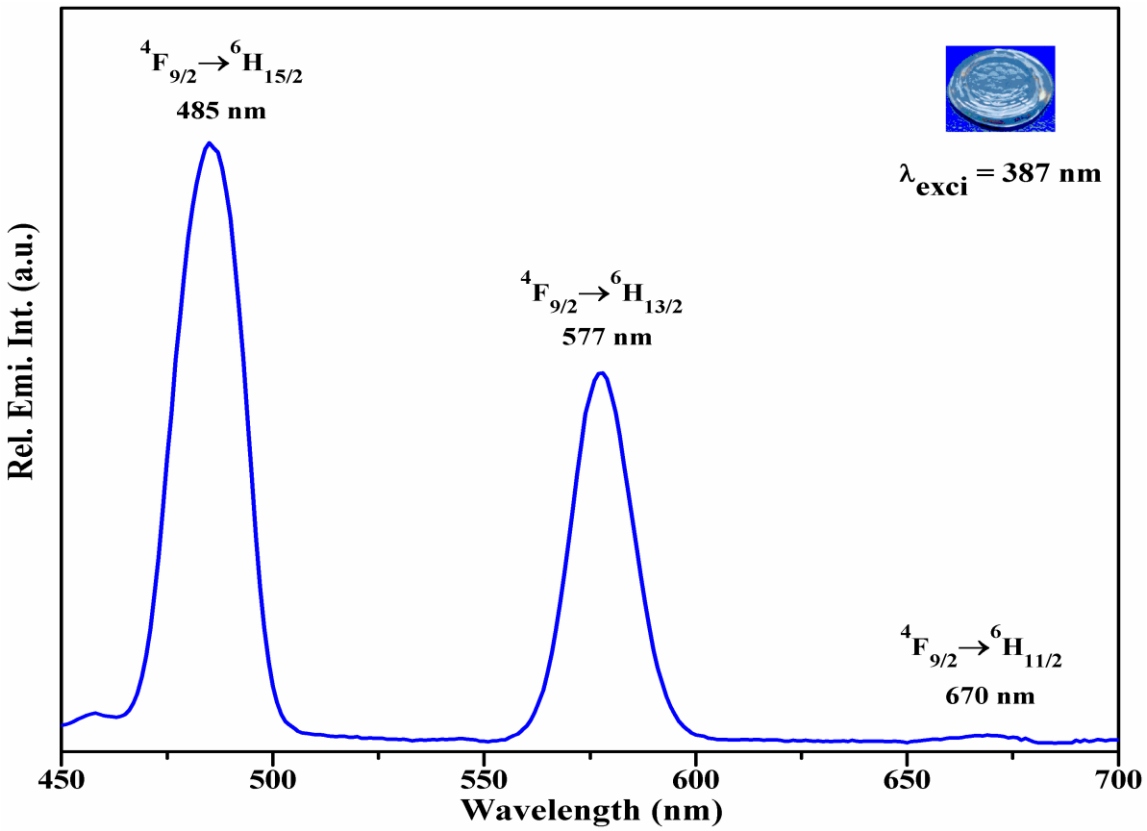

Figure 12